Nano World Journal

https://doi.org/10.17756/nwj.2023-s2-013

Research Article

Open Access

Mineralogy and Stabilization Conditions of Hydroxyapatite Produced from an Alkali-activated Electric Arc Furnace Slag

H. Agourrame*, F. Ouzoun, A. Moussadik, H. Ez-zaki, N. Khachani and A. Diouri*

Faculté des Sciences, Université Mohammed V de Rabat, Avenue Ibn Battouta, BP 1014, Laboratoire de Chimie Appliquée des Matériaux, Rabat, Morocco

***Correspondence to:**
H. Agourrame
Faculté des Sciences,
Université Mohammed V de Rabat,
Avenue Ibn Battouta, BP 1014,
Laboratoire de Chimie Appliquée des Matériaux,
Rabat, Morocco.
E-mail: hind.agourrame@gmail.com

A. Diouri
Faculté des Sciences,
Université Mohammed V de Rabat,
Avenue Ibn Battouta, BP 1014,
Laboratoire de Chimie Appliquée des Matériaux,
Rabat, Morocco.
E-mail: a.diouri@um5r.ac.ma

Received: July 25, 2023
Accepted: September 20, 2023
Published: September 22, 2023

Citation: Agourrame H, Ouzoun F, Moussadik A, Ez-zaki H, Khachani N, et al. 2023. Mineralogy and Stabilization Conditions of Hydroxyapatite Produced from an Alkali-activated Electric Arc Furnace Slag. *NanoWorld J* 9(S2): S75-S80.

Published by United Scientific Group

Abstract

The electric arc furnace slag (EAFS) is a by-product generated during the production of steel in electric arc furnaces. It is a highly versatile material with significant importance in various applications. With its multiple applications and positive environmental impact, EAFS plays a crucial role in sustainable development and resource conservation. The present research focuses on the black slag from SONASID-Jorf steel in Morocco for preparation of Hydroxyapatite (HAP; $(Ca_5(PO_4)_3(OH))$ phase. This phase was successfully synthesized by activated slag with alkali activator NaOH (Sodium hydroxide) and using a wet precipitation method with molar ratio of Ca/P = 1.67. X-ray diffraction (XRD), Fourier transform infrared (FTIR) spectroscopy measurement, scanning electron microscopy (SEM) analysis techniques were performed on the samples to characterize the mineralogical and microstructural properties. The characterization of the developed phases indicates the formation of mixtures of dicalcium silicate with phases of dellaite ($Ca_6Si_3O_{11}(OH)_2$) and fayalite (Fe_2SiO_4) in the black slag activated with alkali activator NaOH. Moreover, indicates the formation of the HAP phases synthesized by wet precipitation method. The micrographs obtained by SEM show the morphology of rod-shaped indicate the presence of HAP phase.

Keywords

Blast furnace slag, Alkali activator, Hydroxyapatite

Introduction

Steelmaking industries are one of the important sources for recovering metals from their wastes. Oxidation of these metals by dissolved oxygen in hot metal is the key reaction in steelmaking industries [1]. Steel slag is a non-metallic solid residue which is produced during steel and iron production in different types of furnaces and contributes to approximately 10 - 15 wt.% of produced steel [2]. Steel slag can be divided into open hearth furnace slag, EAFS, basic oxygen furnace slag, energy optimizing furnace slag, ladle furnace slag, and induction furnace slag [3]. EAFS is produced during crude steelmaking via an EAF steel scrap together with the fluxes of limestone or dolomite is heated to form a liquid phase by means of an electric current [4]. We note that the calcium oxide (CaO) and hematite (Fe_2O_3) contents of basic oxygen furnace slag and EAFS are high, while the CaO content of induction furnace slag is low, indicating that the chemical composition of steel slag of different origins and types is considerably different. The presence of CaO and magnesium oxide (MgO) in steel slag results in lower activity and poor volumetric stability [3]. Disintegration in slags may be due to conversion of unstable polymorphs dicalcium silicate to the low (g) temperature form of calcium silicate (Ca_2SiO_4), which is accompanied by an increase of 10% in volume and leads to disintegration of the slag. To avoid or to neutralize these defects, quick cooling of the slag is necessary [5]. They suggested that there is a

combined effect of the superheat and primary phase on the viscous behavior of slag. In addition, the viscosity of metallurgical slags strongly depends on the potential of dicalcium silicate [6]. The industrial by products could be assumed to be the low-cost adsorbents due to their abundance in nature and less processing requirements. The slag as an alternative adsorbent has been used to remove heavy metals in the environmental field due to its unique properties [7]. Moreover, steel slag has a large specific surface area and porosity, which is a solid waste with good adsorption properties; solid-waste application to water bodies to remove inorganic non-metallic ions, heavy metal ions, radioactive elements, rare metal elements, and organic compounds has achieved better removal results [3]. Alkali-activated materials synthesis can be performed with a quite low energy input, keeping the alkaline activation at low values, and performing the reaction at room temperature, mitigating the release of greenhouse gases. Moreover, they could be reused in other applications after exhaustion when used as sorbents for water depollution [8]. Alkali-activated binders based on ground granulated blast furnace slag represent a viable and sustainable alternative to Portland cement since they use by-products of other industrial manufacturing processes. The easiness of activation and the hydration of the slags depend mainly upon the mineralogical composition and fineness of the slag and on the type of the alkaline activator used. The addition of alkalis stimulates the dissolution of the slag and thus the formation of hydration products, mainly calcium silicate hydrates incorporating significant amounts of aluminium (C(-A)-S-H), hydrotalcite-like phase and strätlingite [9]. Moreover Dellaite phase $Ca_6(Si_2O_7)(SiO_4)(OH)_2$ or $3(Ca_2SiO_4).H_2O$,is a very rare hydrated dicalcium silicate mineral, which was first discovered by Agrell in 1965 in Kilchoan, Scotland. Its synthetic equivalent has been studied as a major phase of calcium silicate hydrate (γ-C_6S_3H in the C-S-H system) in the cement industry [10]. HAP, previously referred to as hydroxylapatite, is a mineral that occurs naturally and is relatively uncommon [11]. Furthermore, chemically known as $Ca_{10}(PO_4)_6(OH)_2$, HAP is a biocompatible, osteoconductive, and bioactive ceramic capable of establishing direct connections with living tissues [12]. Besides, HAP represents the hydroxyl terminal constituent of the apatite group, which possesses a general formula of $M_{10}(RO_4)_6X_2$ [11]. Moreover, the synthesis of HAP with desired properties continues to be a complex task due to the potential formation of harmful intermediate substances during its production [13]. Various approaches have been developed to create HAP, including the dry method, wet method, thermal method, or a combination of these techniques. Additionally, HAP can be derived from natural sources such as mammalian bones, eggshells, and plant materials [14]. HAP is extensively utilized in the field of medicine. It is widely employed as a filler material for mending bone defects, in the production of ceramic implants and coatings for metal implants, in the formulation of bone cements, as drug delivery systems, and as an additive in toothpastes and cleaning agents. Moreover, synthetic HAP acts as a filler for column chromatography and finds utility in gas sensors, catalysts, and sorbents [11]. Recently, it has been used nanometric HAP as filler in dental resins [15]. HAP has been commonly applied in medical and pharmaceutical field due to its excellent biocompatibility. Besides, it's also widely applied in adsorption process owing to the adsorption feature, particles and porous granules of HAP possess [16]. HAP is alkaline in nature and used in adsorption and catalysis [17]. However, HAP has a powerful ion exchange capacity and surface adsorption properties under various redox conditions and has been extensively used in the adsorption and removal of heavy metals and inorganic-organic pollutants, protein purification, and catalytic or loading catalysts [18]. In a recent study the HAP-zeolite composite material (HAP-ZE) material has a great adsorption performance in removing Mn^{2+}, NH^{4+}, and phosphate ions mixed in water, on grounds of the higher ion-exchange capacities and abundantly existing Ca^{2+} ions in HAP-ZE structure [16]. The objective of this work was to synthesis HAP phase using EAFS as adsorbents for the removal of crystal violet in water. The surface structure of the materials was investigated by means of XRD, FTIR spectroscopy measurement, SEM analysis techniques were performed on the samples to characterize the mineralogical and microstructural properties.

Materials and Method

In this study, synthesis of HAP phase is conducted in this manner: In order to achieve higher dissolution performance, the EAFS was ground and sifted with a < 40µm sieve before synthesis. First, the ratio of EAFS to NaOH was mixed at 1:1.3 (wt.%) to ensure a consistent mixture. What follows is to heat the mixture in a ceramic container at 600 °C for 90 min. The sample activated with NaOH is named SBN (Black slag). After that the product cool down and crush it. Afterward, a 5.0 g of the fusion product powder was taken and dissolved in 30 ml of 2.0 mol/L NaH_2PO_4 aqueous solution until homogenized. Once dissolution is completed, another 50 ml of 3.0 mol/L NaOH aqueous solution was added drop by drop into the above suspension. It should be noted that the Ca/P molar ratio of the suspension was fixed at 1.7, the obtained slurry was vigorously stirred for 2 h at 100 °C, subsequently aged at the same temperature for a certain time without stirring to achieve crystallization. At the end of the process the solid phase was collected by filtration, washed several times with distilled water, and then dried at 80 °C. Sample prepared with the NaH_2PO_4 is named respectively SBNP (Black slag). HAP with nanoproperties.

Results and Discussion

X-ray fluorescence

The chemical composition of Blast Furnace Slag (BFS) exhibits similarity across different regions, indicating minimal variation [19]. This similarity plays a significant role in the widespread utilization of BFS. Research conducted by other authors on the chemical compositions of EAFS reveals that the most common chemical compounds found in EAFS include iron oxides such as wüstite (FeO) and Fe_2O_3, CaO, silicon dioxide (SiO_2), aluminum oxide (Al_2O_3), MgO, manganese oxide (MnO), and chromium oxide (Cr_2O_3) [19]. The composition of BFS is primarily influenced by the source of iron ore and the smelting process, resulting in some degree of variation within a certain range [19]. Notably, FeO and CaO

are the main compounds present in the slag [20]. The most recent research demonstrates that the oxides CaO, MgO, and Al_2O_3 play a significant role in enhancing the hydraulic reactivity of slags, contributing to increased chemical cementation when water, lime, and other materials are introduced [21]. Another study reveals that BFS primarily consists of alkaline oxides CaO and MgO, as well as acidic oxides Al_2O_3 and SiO_2. The content of CaO ranges from 35.8% to 43.9%, MgO ranges from 7.4% to 13%, Al_2O_3 ranges from 6.2% to 12.5%, and SiO_2 ranges from 32.4% to 36.2% [19]. Among the slag materials reported in the literature, the highest calcium content observed is 40.46% by mass, which is utilized for lead (II) adsorption [22]. Other study shows that the geopolymer synthesis a had conducted by used ground granulated blast furnace slag, an industrial by-product, as a material source [23]. The average content of calcium as oxide (CaO) in BFS was approximately 46.62%, making it the main element, followed by Si, Ba, Mn, and Mg [24]. The highest CaO content (50.37%) in the slag material is attributed to the use of limestone during slag production to eliminate impurities from the iron ore reduction process [23]. The chemical composition of the BFS used in the present study was investigated by X-ray fluorescence, results are listed in table 1. The slag was mainly composed of CaO, Al_2O_3, Fe_2O_3, and SiO_2 components.

Table 1: Chemical composition of the black slag sample Sonasid-Jorf.

Oxides	SB (< 40µm)
SiO_2	10.62
Al_3O_3	6.37
Fe_2O_3	25.4
CaO	23.88
MgO	5.04
SO_3	0.29
K_2O	0.01
TiO_2	0.50
MnO	3.07
P_2O_5	0.38
SrO	0.083
LOI	23.75

X-ray diffraction

Figure 1 shows the XRD diagram of the black slag. The analyzes show that the main crystallized phases identified in the black slag (SB) are Ca_2SiO_4. And mainly consists of the crystallized phases: FeO, MgO, Ca_2SiO_4, Fe_2SiO_4. The intensities of the characteristic diffraction peaks of Ca_2SiO_4 phase are less in the black slag. This is mainly due to the black slag which probably contains vitrified or amorphous compounds. Furthermore, the presence of dicalcium silicate (C_2S) is the preferred phase in slag from the observed peak intensity, which shows that the C_2S phase is the main constituent in slag [25].

Figure 2 show the XRD pattern of the black slag alkali activated with NaOH. The analysis shows that the dicalcium silicate (β-Ca_2SiO_4) phase identified in the SBN of the monoclinic crystal system metastable at room temperature [26]. It is clear that the crystallinity of the synthesized composite sample was influenced by the NaOH concentration of the initial mixture. The black slag in the figure 3 (SBN) mainly consists of the crystallized phases are dellaite and fayalite. Dellaite was first discovered by Agrell (1965, Mineral. Mag) at Kilchoan, Scotland, in a metamorphosed limestone. It has further been synthesized as a major calcium silicate hydrate phase in the C-S-H system in the cement industry. The unit cell was refined as triclinic from the powder diffraction data, with a = 6.815(4), b = 6.937(3), c = 12.890(6) Å, α = 90.71(4), β = 97.68(4), γ = 98.20(4)°, and V = 597.4(5) Å3 [27]. Dellaite is a crystalline calcium silicate hydrate with a C/S ratio of 2. The presence of this phase has been previously reported in geothermal cements [27]. Furthermore, fayalite is a common member of the olivine group of minerals. Olivine is a name for a series of silicate minerals with the formula M_2SiO_4, where M is most commonly Fe or Mg. Olivine has an orthorhombic structure. The structure consists of isolated SiO^{4-} tetrahedra, which are held together by M cations occupying two types of octahedral site (M1 and M2) [29]. The XRD pattern (SBNP) for 2 h of aging showed several diffraction peaks assignable to HAP phase in black slag. HAP is a natural crystalline mineral and has a Ca/P ratio of 1.67 [30]. Two types of HAP crystal structures have been described: a monoclinic form, defined by the P21/b space group (Z = 4), and a hexagonal form, defined by the P63/m space group (Z = 2) [30]. Hexagonal HAP has a disordered hydroxyl arrangement along the c-axis and the

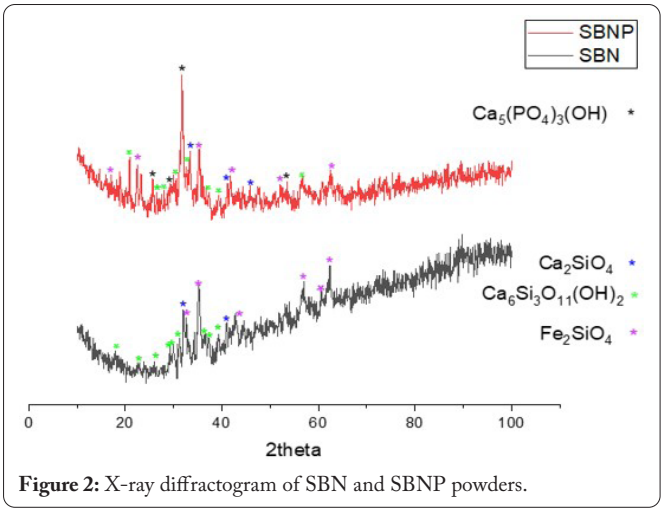

Figure 2: X-ray diffractogram of SBN and SBNP powders.

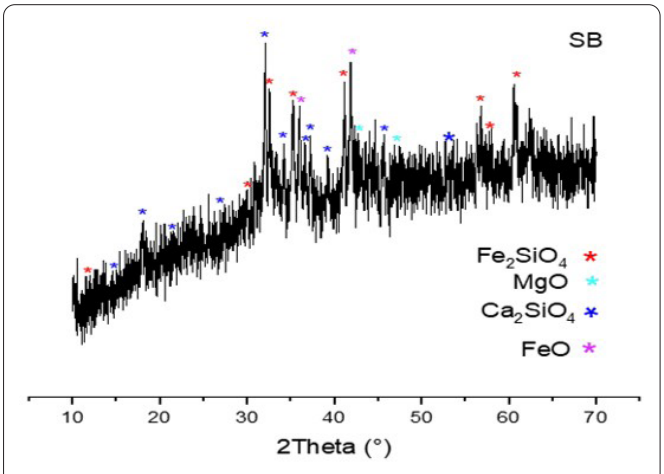

Figure 1: X-ray diffractogram of SBN powder.

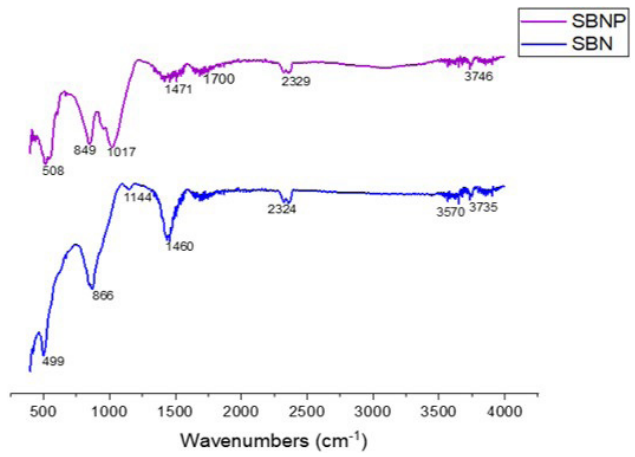

Figure 3: FTIR Spectrum of SBNP and SBN powders.

hydroxyl ions are pointed in upper and lower directions. In contrast, monoclinic HAP (space group P21/b) has an ordered hydroxyl arrangement along the c-axis, and hydroxyl ions are aligned in the same direction on the hydroxyl columns [31]. The unit cell parameters of the monoclinic structure are a = 9.84214 Å, b = 2a, c = 6.8814 Å, and γ = 120°. An important characteristic of this form is that it can be easily destabilized by the presence of foreign ions. The lattice parameters of the hexagonal structure are as follows: a = b = 9.418 Å, c = 6.884 Å, α = β = 90°, and γ = 120°. In this structure, calcium cations can be located at two different sites, Ca1 and Ca2 [30].

FTIR spectroscopy

The FTIR spectrum of the (SBN-SBNP) powders is presented in figure 3. The majority of the detected absorption bands correspond to the polymorph of the dicalcium silicate α-Ca_2SiO_4 are located around 800 - 1000 cm^{-1} [32]. The absorption bands located at 1431 cm^{-1} - 1460 cm^{-1} correspond to the Ca-O bond [33]. Due to the presence of humidity in the air. In general, the zones from 500 to 800 cm^{-1} are identified as corresponding respectively to the deformations of the stretching and bending bands of Si-O [34]. The bands observed in the FTIR spectra of figure 3 in SBN phase show the ν3 stretching for the peak of Fe-Si-O at 866.86 cm^{-1} still existed, suggesting that Fe_2SiO_4 did not resolve completely, which was consistent with the results of XRD [35]. The band at 3573 cm^{-1} corresponds to the hydroxyl groups [36]. Very broad bands for molecular water at about 3300 - 3600 cm^{-1} (OH stretch) [37]. Finally, two bands relating to vibration of the adsorbed water in apatite lattice could be noticed as a broad peak between 3600 and 3000 cm^{-1} [38].

Scanning electron microscopy

SEM (JSM-7000F FE-SEM) is used to study the morphology of samples and obtain information on crystal shape, size, and grain texture. SEM micrographs of the SBN sample are shown in figure 4a. They show the morphology of dellaite was crystallized to large bulky crystals [39]. Moreover, the presence of C-S-H flowery-like morphology is found in the sample as it is the by-product from the cement hydration [40]. Consistent with our SEM observations, the fayalite particles are found to adopt irregular shape, and have poorly defined crystallographic facets [41]. SEM micrographs of the SBNP sample are shown in figure 4b. The ultra-long sheet-like observed of rod-shaped [42] indicates the presence of HAP [43]. Furthermore, HAP exhibits whiskers with a hexagonal structure [44], on this latter we find various morphologies, including plate-like and needle-like. These forms are the morphologies of the HAP phase [45].

Conclusion

In this study, the objective was to synthesis HAP phase using EAFS as adsorbents for the removal of crystal violet in water. The results of this study can be summarized as follows: XRD results showed that the dellaite and fayalite phases could be clearly observed with activator NaOH. HAP composite material was successfully synthesized from EAFS with a fusion method involving alkaline fusion and a wet precipitation method treatment in this research. The HAP phase synthesized by wet precipitation method gives morphology like rod-shaped. The identified composite has good prospects as absorbents to remove contaminants.

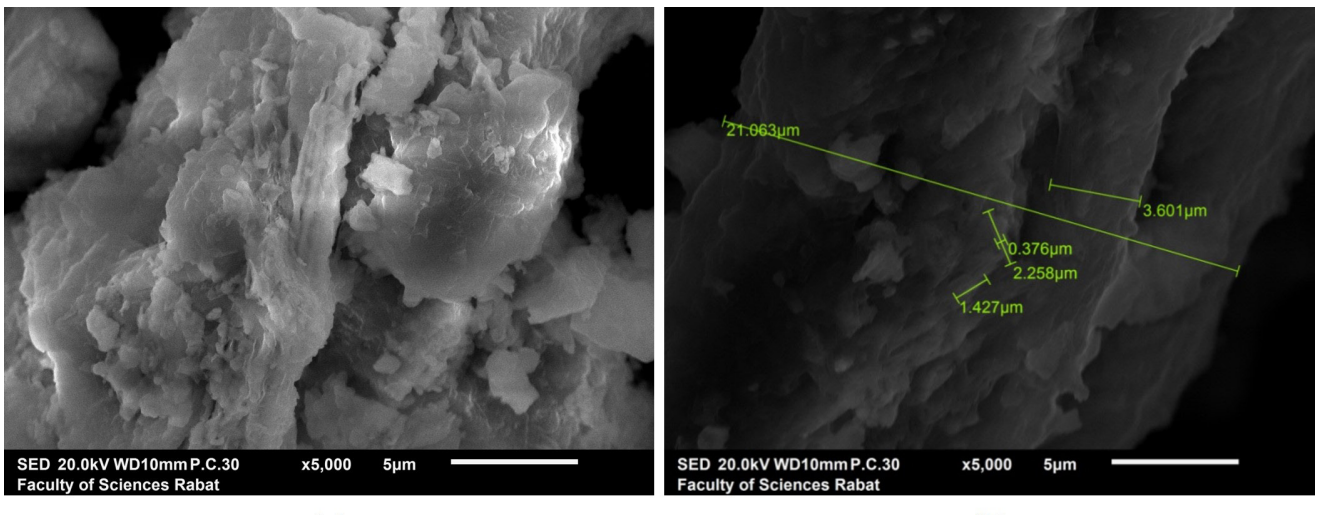

Figure 4: SEM image of **(a)** SBN and **(b)** SNBP samples x5000.

Acknowledgments

None.

Conflict of Interest

None.

References

1. Turkdogan ET. 1984. Physicochemical aspects of reactions in ironmaking and steelmaking processes. *Trans Iron Steel Inst Japan* 24(8): 591-611. https://doi.org/10.2355/isijinternational1966.24.591
2. Proctor DM, Fehling KA, Shay EC, Wittenborn JL, Green JJ, et al. 2000. Physical and chemical characteristics of blast furnace, basic oxygen furnace, and electric arc furnace steel industry slags. *Environ Sci Technol* 34(8): 1576-1582. https://doi.org/10.1021/es9906002
3. Shi C, Wang X, Zhou S, Zuo X, Wang C. 2022. Mechanism, application, influencing factors and environmental benefit assessment of steel slag in removing pollutants from water: a review. *J Water Process Eng* 47: 102666. https://doi.org/10.1016/j.jwpe.2022.102666
4. Alsheyab MA, Khedaywi TS. 2013. Effect of electric arc furnace dust (EAFD) on properties of asphalt cement mixture. *Resour Conserv Recycl* 70: 38-43. https://doi.org/10.1016/j.resconrec.2012.10.003
5. Luxán MP, Sotolongo R, Dorrego F, Herrero E. 2000. Characteristics of the slags produced in the fusion of scrap steel by electric arc furnace. *Cem Concr Res* 30(4): 517-519. https://doi.org/10.1016/S0008-8846(99)00253-7
6. Lee S, Min DJ. 2018. Viscous behavior of FeO-bearing slag melts considering structure of slag. *Steel Res Int* 89(8): 1800055. https://doi.org/10.1002/srin.201800055
7. Rađenović A, Malina J, Sofilić T. 2013. Characterization of ladle furnace slag from carbon steel production as a potential adsorbent. Adv *Mater Sci Eng* 2013: 198240. https://doi.org/10.1155/2013/198240
8. Latorrata S, Balzarotti R, Adami MI, Marino B, Mostoni S, et al. 2021. Wastewater treatment using alkali-activated-based sorbents produced from blast furnace slag. *Appl Sci* 11(7): 2985. https://doi.org/10.3390/app11072985
9. Haha MB, Lothenbach B, Le Saout GL, Winnefeld F. 2011. Influence of slag chemistry on the hydration of alkali-activated blast-furnace slag—part I: effect of MgO. *Cem Concr Res* 41(9): 955-963. https://doi.org/10.1016/j.cemconres.2011.05.002
10. Shimazaki H, Miyawaki R, Yokoyama K, Matsubara S, Bunno M. 2008. Occurrence and new data of dellaite from the Akagane mine, Japan. *J Min Petrol Sci* 103(6): 385-389. https://doi.org/10.2465/jmps.080214
11. Bulina NV, Makarova SV, Baev SG, Matvienko AA, Gerasimov KB, et al. 2021. A study of thermal stability of hydroxyapatite. *Minerals* 11(12): 1310. https://doi.org/10.3390/min11121310
12. Lara-Ochoa S, Ortega-Lara W, Guerrero-Beltrán CE. 2021. Hydroxyapatite nanoparticles in drug delivery: physicochemistry and applications. *Pharmaceutics* 13(10): 1642. https://doi.org/10.3390/pharmaceutics13101642
13. Pu'ad NM, Koshy P, Abdullah HZ, Idris MI, Lee TC. 2019. Syntheses of hydroxyapatite from natural sources. *Heliyon* 5(5): e01588. https://doi.org/10.1016/j.heliyon.2019.e01588
14. Abdul Halim NA, Hussein MZ, Kandar MK. 2021. Nanomaterials-upconverted hydroxyapatite for bone tissue engineering and a platform for drug delivery. *Int J Nanomed* 16: 6477-6496. https://doi.org/10.2147/IJN.S298936
15. Moreno-Vargas YA, Luna-Arias JP, Flores-Flores JO, Orozco E, Bucio L. 2017. Hydration reactions and physicochemical properties in a novel tricalcium-dicalcium silicate-based cement containing hydroxyapatite nanoparticles and calcite: a comparative study. *Ceram Int* 43(16): 13290-13298. https://doi.org/10.1016/j.ceramint.2017.07.027
16. Li C, Li X, Yu Y, Zhang Q, Li L, et al. 2022. A novel conversion for blast furnace slag (BFS) to the synthesis of hydroxyapatite-zeolite material and its evaluation of adsorption properties. *J Ind Eng Chem* 105: 63-73. https://doi.org/10.1016/j.jiec.2021.08.017
17. Khanday WA, Hameed BH. 2018. Zeolite-hydroxyapatite-activated oil palm ash composite for antibiotic tetracycline adsorption. *Fuel* 215: 499-505. https://doi.org/10.1016/j.fuel.2017.11.068
18. Huang J, Liu T, Zhang Y, Hu P. 2022. Internal coordination of vanadium industrial waste—preparation of hydroxyapatite and fluorine wastewater purification. *J Water Process Eng* 49: 103041. https://doi.org/10.1016/j.jwpe.2022.103041
19. Zhang L, Jia Y, Shu H, Lu X, Bai F, et al. 2021. The effect of basicity of modified ground granulated blast furnace slag on its denitration performance. *J Clean Prod* 305: 126800. https://doi.org/10.1016/j.jclepro.2021.126800
20. Rojas YP, López EV, Díaz RO. 2021. Morphological, chemical, and mineralogical characterization of concrete mixtures produced by electric arc furnace slag. *J Phys Conf Ser* 2046(1): 012035. https://doi.org/10.1088/1742-6596/2046/1/012035
21. Kambole C, Paige-Green P, Kupolati WK, Ndambuki JM, Adeboje A. 2019. Comparison of technical and short-term environmental characteristics of weathered and fresh blast furnace slag aggregates for road base applications in South Africa. *Case Stud Constr Mater* 11: e00239. https://doi.org/10.1016/j.cscm.2019.e00239
22. Gill B, Martínez-Pavetti B, Monteiro M. 2020. Chemical and microstructural characterization of blast furnace slag. *Rev Soc Cient Paraguay* 25(2): 101-110.
23. Aziz IH, Abdullah MM, Salleh MM, Azimi EA, Chaiprapa J, et al. 2020. Strength development of solely ground granulated blast furnace slag geopolymers. *Constr Build Mater* 250: 118720. https://doi.org/10.1016/j.conbuildmat.2020.118720
24. Abdelbasir SM, Khalek MA. 2022. From waste to waste: iron blast furnace slag for heavy metal ions removal from aqueous system. *Environ Sci Pollut Res* 29(38): 57964-57979. https://doi.org/10.1007/s11356-022-19834-3
25. Chang KL, Huang CT, Huang W, Liu YC. 2008. Investigations of microstructure and phosphorus distribution in BOF slag. *China Steel Tech Rep* 21: 1-6.
26. Midgley CM. 1952. The crystal structure of β dicalcium silicate. *Acta Cryst* 5(3): 307-312. https://doi.org/10.1107/S0365110X52000964
27. Cámara F, Gagne OC, Uvarova Y, Belakovskiy DI. 2016. New mineral names. *Am Min* 101(9): 2123-2131. https://doi.org/10.2138/am-2016-NMN101916
28. Tantawy MA, Shatat MR, El-Roudi AM, Taher MA, Abd-El-Hamed M. 2014. Low temperature synthesis of belite cement based on silica fume and lime. *Int Sch Res Notices* 2014: 873215. https://doi.org/10.1155/2014/873215
29. Kurashina K, Kurita H, Kotani A, Takeuchi H, Hirano M. 1997. In vivo study of a calcium phosphate cement consisting of α-tricalcium phosphate/dicalcium phosphate dibasic/tetracalcium phosphate monoxide. *Biomaterials* 18(2): 147-151. https://doi.org/10.1016/S0142-9612(96)00173-1
30. De Lama-Odría MD, Valle LJ, Puiggalí J. 2023. Lanthanides-substituted hydroxyapatite for biomedical applications. *Int J Mol Sci* 24(4): 3446. https://doi.org/10.3390/ijms24043446
31. Mostafa NY, Brown PW. 2007. Computer simulation of stoichiometric hydroxyapatite: structure and substitutions. *J Phys Chem Solids* 68(3): 431-437. https://doi.org/10.1016/j.jpcs.2006.12.011
32. Mollah MY, Tsai YN, Hess TR, Cocke DL. 1992. An FTIR, SEM and EDS investigation of solidification/stabilization of chromium using portland cement Type V and Type IP. *J Hazard Mater* 30(3): 273-283. https://doi.org/10.1016/0304-3894(92)87004-Y
33. Nochaiya T, Sekine Y, Choopun S, Chaipanich A. 2015. Microstructure, characterizations, functionality and compressive strength of ce-

ment-based materials using zinc oxide nanoparticles as an additive. *J Alloys Compd* 630: 1-10. https://doi.org/10.1016/j.jallcom.2014.11.043

34. Wang S, Peng X, Tang L, Zeng L, Lan C. 2014. Influence of inorganic admixtures on the 11 Å-tobermorite formation prepared from steel slags: XRD and FTIR analysis. *Constr Build Mater* 60: 42-47. https://doi.org/10.1016/j.conbuildmat.2014.03.002
35. Zhang S, Zhu N, Mao F, Zhang J, Huang X, et al. 2021. A novel strategy for harmlessness and reduction of copper smelting slags by alkali disaggregation of fayalite (Fe_2SiO_4) coupling with acid leaching. *J Hazard Mater* 402: 123791. https://doi.org/10.1016/j.jhazmat.2020.123791
36. Zhao X, Liu Q, Yang J, Zhang W, Wang Y. 2018. Sintering behavior and mechanical properties of mullite fibers/hydroxyapatite ceramic. *Materials* 11(10): 1859. https://doi.org/10.3390/ma11101859
37. Fleet ME, Liu X. 2008. Accommodation of the carbonate ion in fluorapatite synthesized at high pressure. *Am Min* 93(8-9): 1460-1469. https://doi.org/10.2138/am.2008.2786
38. Sharifnabi A, Fathi MH, Yekta BE, Hossainalipour M. 2014. The structural and bio-corrosion barrier performance of Mg-substituted fluorapatite coating on 316L stainless steel human body implant. *Appl Surf Sci* 288: 331-340. https://doi.org/10.1016/j.apsusc.2013.10.029
39. Yanagisawa K, Hu X, Onda A, Kajiyoshi K. 2006. Hydration of β-dicalcium silicate at high temperatures under hydrothermal conditions. *Cem Concr Res* 36(5): 810-816. https://doi.org/10.1016/j.cemconres.2005.12.009
40. Sutan NM, Yakub I, Jaafar MS, Matori KA, Sahari SK. 2015. Sustainable nanopozzolan modified cement: characterizations and morphology of calcium silicate hydrate during hydration. *J Nanomat* 2015: 713258. https://doi.org/10.1155/2015/713258
41. Qafoku O, Ilton ES, Bowden ME, Kovarik L, Zhang X, et al. 2018. Synthesis of nanometer-sized fayalite and magnesium-iron (II) mixture olivines. *J Colloid Interface Sci* 515: 129-138. https://doi.org/10.1016/j.jcis.2018.01.036
42. Zhu K, Yanagisawa K, Onda A, Kajiyoshi K, Qiu J. 2009. Morphology variation of cadmium hydroxyapatite synthesized by high temperature mixing method under hydrothermal conditions. *Mater Chem Phys* 113(1): 239-243. https://doi.org/10.1016/j.matchemphys.2008.07.049
43. Xia W, Lin K, Gou Z, Engqvist H. 2012. Morphology Control of Hydroxyapatite Crystal and Its Aggregates. In Gshalaev VS, Demirchan AC (eds) Hydroxyapatite Synthesis, Properties and Applications. Nova Science Publishers, pp 243-265.
44. Szterner P, Antosik A, Pagacz J, Tymowicz-Grzyb P. 2023. Morphology control of hydroxyapatite as a potential reinforcement for orthopedic biomaterials: the hydrothermal process. *Crystals* 13(5): 793. https://doi.org/10.3390/cryst13050793
45. Tomozawa M, Hiromoto S. 2011. Microstructure of hydroxyapatite-and octacalcium phosphate-coatings formed on magnesium by a hydrothermal treatment at various pH values. *Acta Mater* 59(1): 355-363. https://doi.org/10.1016/j.actamat.2010.09.041